CLM-P 401

QUANTITATIVE X-RAY SPECTROSCOPY OF THE LIGHT-ABSORPTION REGION AT THE SURFACE OF LASER-IRRADIATED POLYETHYLENE

by

M Galanti† and N J Peacock

(Submitted for publication in J.Phys. B, Atom.Molec.Phys.)

ABSTRACT

Absolute X-ray spectroscopic measurements of the lines and continua from space-resolved C^{6+}, C^{5+}, C^{4+}, C^{3+} ions at the surface of a plane polyethylene target, irradiated by a 1.06 micron neodymium laser, are interpreted in terms of a collisional-radiative model in which some of the allowed lines are optically thick. The degree of ionisation increases monotonically with laser power density over the range 10^{11} to 2×10^{12} watts cm^{-2} and the electron energy distributions are strictly Maxwellian. The ion population ratios indicate that the ionisation time is of the order of 1 to 10 picoseconds and is limited by thermal expansion within a thin layer whose mean density is $\sim 3 \times 10^{21}$ cm^{-3}.

† EURATOM Fellow - On attachment from Imperial College, London.

Euratom-UKAEA Association for Fusion Research,
Culham Laboratory,
Abingdon, Oxon,
OX 14 3DB, UK.

September 1974

1. INTRODUCTION

The plasma produced by irradiation of solid targets with high-intensity laser beams is of considerable topical interest. Calculations by Nuckolls et al (1972) have demonstrated that, with appropriate time-variation in intensity and symmetry of irradiation, compression to densities greatly exceeding that of the solid state is possible and could lead to thermonuclear fusion using targets of fusionable light elements. The generation of highly-stripped ions in laser-produced plasmas is also of wide interest in astrophysics, see eg. Fawcett, Galanti and Peacock (1974), in atomic structure studies, Peacock, Hobby and Galanti (1973) and also as a possible source of heavy ions, Peacock and Pease (1969).

The mechanism for absorption of the laser light and the physical processes resulting from the rapid deposition of the laser energy are both wavelength and intensity-dependent and are critical problems in the above applications. Several models for the energy-balance and plasma dynamics of the laser beam-target interaction have been described in the literature eg. Caruso and Gratton (1968), Krokhin (1971), Floux (1971), Bobin (1971).

This paper reports on quantitative measurements of the plasma parameters in the radiant-energy absorption-layer at the surface of a plane polyethylene target which is irradiated by a focussed, multigigawatt, neodymium-laser beam. Space-resolved, spectroscopic measurements of the emission from the carbon ions, especially the free-bound continua from C^{6+} and C^{5+}, are used to deduce the variation in the plasma density and temperature with distance from the target surface. The intensity distribution of the photons emitted with energies less than 3 keV is recorded directly on a grazing-incidence spectrograph which has been absolutely calibrated for intensity against wavelength, Hobby and Peacock (1973), Irons and Peacock (1973).

The derivation of the temperature from the dispersed continuum offers some advantages over the absorber foil technique in that the effect of impurities,

overlapping continua and non Maxwellian distributions (Galanti, Peacock et al(1974)),are more easily accounted for. The electron density is derived from the absolute intensities of the free-bound continua.

A study has also been made of the relative ion populations in the absorption layer. The relative populations of C^{6+} to C^{5+} ions are directly proportional to the intensities of the free-bound continua associated with each ion. The ratio of the populations of C^{4+} to C^{3+} ions can be derived from the intensities of the intercombination and satellite lines which are located at slightly longer wavelength than the CV allowed resonance lines. These satellite emission lines are distinctive features of the absorption layer (Peacock, Hobby and Galanti 1973).

The ion populations are related to the plasma parameters through the density and temperature-dependent ionisation and recombination rates. They are also dependent on the ion transit time through the absorption layer. From the spectroscopic measurements therefore, the ion transit time and the dimensions of the high temperature plasma layer have been deduced. The results can be interpreted most appropriately in terms of a model where an appreciable fraction, ~ 30%, of the radiant energy is entirely absorbed at the critical density, which for 1.06 μm radiation is 1×10^{21} cm^{-3}.

Comparison of the experimental results with the predictions of 1-dimensional numerical hydrodynamic code developed by Ashby and Christiansen (1973), Christiansen, Ashby and Roberts (1973), indicate that for our experimental conditions of a 4.5 nsec long laser pulse and a focal area at the target whose diameter is 300 μm, a quasi-stationary plasma layer is formed with the critical density close to the original target surface. The time-averaged, but spatially-resolved values for the plasma parameters therefore give a reasonable description of the light-absorption region. Furthermore, since the focussed light intensity does not exceed 5×10^{12} watts cm^{-2}, absorption by non-linear processes such as described by Kruer and Dawson (1972) are not expected to influence the plasma dynamics.

Previous communications, eg. Donaldson, Hutcheon and Key (1973),

Colombant and Tonon (1973), on the ionisation state in laser-produced plasmas have relied on simple model-calculations whereas in our present work the ion populations are measured directly and consideration is given to the distribution of electrons within the excited bound states. The conclusions we draw from our work are also significantly different from these previous publications.

2. EXPERIMENTAL METHOD

A 4.5 nanosec pulse was switched out of a neodymium laser oscillator operating in the pulse transmission mode, and amplified in three stages to a power, averaged over the pulse half-intensity width, of 4 gigawatts. The output beam was focussed via a 10 cm focal length, 2-element lens onto a plane target of solid polyethylene, $(CH_2)_n$, in vacuo. The focal spot was located 4 mm from the entrance slit of a 2 metre grazing-incidence grating spectrograph. In the present experiments, the laser light intensity at the target was varied over the range 10^{11} to 2×10^{12} watts cm^{-2} with a focal spot diameter of 300 microns. Modulation of the laser intensity, observed using a 30 picosecond resolution streak camera, was less than 20%. The radiation from the plasma, transmitted through the 5 micron wide horizontal entrance slit of the spectrograph and incident on the grating at a 2^o grazing angle, was stopped down by a vertical slit, which was located mid-way between the entrance slit and the pole of the grating, see Figure 1a. In this way the spectrum is space-resolved orthogonal to the dispersion and it is possible to discriminate between various temperature and density regions of the plasma. A similar arrangement has been used by Irons and Peacock (1974), to measure recombination rates in the coronal plasma region a few mm from the target surface.

Figure 2 shows part of the CVI and CV emission spectrum from a polyethylene target which has, for ease of illustration, a space-resolution of $\sim$ 100 microns. It is readily seen that in contrast to series of singly-excited lines such as the Lyman lines, the satellite lines are spatially coincident only with the intense free-bound continua at the target surface and it is this region which will be discussed mainly in this paper. The vertical slit was normally 50 microns wide in this study and this is to be taken as the space resolution unless stated otherwise.

The plasma depth was measured from X-ray pin-hole photography of the continuum, between 8 Å and 16 Å, transmitted through a 10 micron thick aluminium foil. Even with our highest resolution, 50 micron, pin-hole aperture, the dimension of the intense continuum at the target surface was limited by the pin-hole size used, and evidently the thickness of the hot, dense, plasma region where the emitted radiant energy reaches a maximum, is considerably less than 50 microns. Again unless otherwise stated the analysis will refer to this spatial region.

3. ELECTRON ENERGY DISTRIBUTIONS FROM THE FREE-BOUND CONTINUA

The electron temperature was measured from the intensity of the electron recombination into the CVI and CV ions. In order to measure the intensity of the continuum, plate density has to be converted to intensity incident on the spectrograph slit over the wavelength region of interest. For temperature measurement a relative calibration is sufficient since the temperature depends only on the slope of the continuum intensity versus wavelength: an absolute calibration allows us to measure the electron and ion density. The spectrograph sensitivity has been evaluated previously, over the region 45 Å to 5 Å, Hobby and Peacock (1973), from measurements of the absolute efficiency of the grating (Bausch and Lomb catalogue No 55-52-40-400, serial No 2278-30-2-6) and the response of the recording emulsion (Ilford Q2 plates). The sensitivity of the same instrument as a complete unit was also measured using the branching ratio technique applied to a similar laser-produced plasma, Irons and Peacock (1973). For the same grating the energy distribution between first, second and third orders has been measured on the grating test facility at Imperial College, R J Speer (1970, 72) so that it is possible to take into account overlapping order effects in estimating the separate continua intensities.

At wavelengths shorter than the ionisation limits and in the temperature range of interest here, the intensity of the free-bound continua ($\alpha\ Z_i^4$) exceeds that of the free-free-continuum ($\alpha\ Z_i^2$), where Z is the ion charge. Expressions for both continua are given in the literature eg. Stratton (1965). viz.,

$$\varepsilon(\nu)_{f-b} = \left(\frac{\chi_H}{KT_e}\right)^{3/2} C' N_e N_i \left(\frac{\chi_{i,n}}{\chi_H}\right)^2 \frac{\xi n}{n} g_{bf} \exp\left[(\chi_i - h\nu)/kT_e\right] \quad \ldots(1)$$

and

$$\varepsilon(\nu)_{f-f} = \sum_{Z_i=Z-2}^{Z} C' N_e N_i Z_i^2 \left(\frac{\chi_H}{kT_e}\right)^{\frac{1}{2}} g_{ff} \exp\left[-h\nu/kT_e\right] \quad \ldots(2)$$

where $C' = 1.7 \times 10^{-40}$ ergs cm^3

χ_H = ionisation potential of the hydrogen atom

$\chi_{i,n}$ = ionisation potential of $C^{Z=i}$ from level n

ξ = number of places in the n^{th} shell which can be filled by the recombining electron

g_{bf} and g_{ff} are free-bound and free-free Gaunt factors.

The sum of the continua intensities with frequency is shown in Figure 3. The energy interval over which the free-bound continua falls by e^{-1} is simply the electron temperature provided the electrons have a Maxwellian distribution. From the ionisation limit at 490 eV out to 2.5 keV (about the limit of the spectrograph sensitivity) the intensity of free-bound continua due to electron recombination into the ground state of CVI, Figure 3, is in good accord with a thermal energy distribution for the free electrons. For the laser flux intensity appropriate to Figure 3, the corresponding temperature is 170 eV ± 20 eV, the error covering the maximum and minimum possible slopes. The CV and CVI continua appear to give the same temperature.

A characteristic of collisionless, non-linear absorption of radiant energy, Kaw and Dawson (1969) is the presence of a high energy-tail to the electron energy distribution. No evidence for non-Maxwellian effects, even up to energies of 50 keV, was detected using scintillator-photomultiplier, high energy detectors. This technique of coupling the continuum recorded on the spectrograph up to 2.5 keV with results from higher energy detectors could be a powerful method of investigating non-linear absorption which should become important at rather higher flux intensities than those studied here.

4. MEASUREMENT OF THE ELECTRON DENSITY

From measurements of absolute recombination intensity into C^{6+} or C^{5+} the products $N_e \cdot N(C^{6+})$ and $N_e \cdot N(C^{5+})$ may be derived according to equation (1).

Let $E(\lambda)$ (ergs $\mathring{A}^{-1}$ ster $^{-1}$) be the energy emitted by the plasma source. The density at the photographic plate is then

$$D(\lambda) = E(\lambda) \frac{d\lambda}{dx} \frac{S(\lambda)}{r_1 r_2} \qquad \ldots(3)$$

where,

$S(\lambda)$ (density erg^{-1} cm^3) is the sensitivity of the instrument. The value of $S(\lambda)$ measured by Hobby and Peacock (1973) has to be decreased by a factor of 2 to take into account a reduction in the slit width by the same factor.

$\frac{dx}{d\lambda}$ is the linear dispersion

r_1 is the distance of the entrance slit from the plasma

r_2 is the distance of the recorded wavelength from the plasma

then; $\varepsilon(\lambda) = \frac{4\pi}{V t} D(\lambda) \frac{dx}{d\lambda} \cdot \frac{r_1 r_2}{S(\lambda)}$, ergs. cm^{-3}sec^{-1}.A^{o-1} .

where V is the plasma volume accommodated by the spectrograph and t is the emission time of the X-rays, measured with a scintillator and photomultiplier. The volume V is estimated from the plasma dimension along the line of sight Z measured from the X-ray pinhole pictures and from Δy and Δx , calculated from the geometrical optics of the instrument slits, Figure 1 (a) and (b).

N_e may be derived from charge neutrality:

$$N_e = [\, 8 + 7\,\alpha + 6\beta + \ldots \,]\, N(C^{6+}) \qquad \ldots(4)$$

assuming two hydrogen ions for each carbon ion in the polyethylene plasma,

where $\alpha = \frac{N(C^{5+})}{N(C^{6+})}$; $\beta = \frac{N(C^{4+})}{N(C^{6+})}$ etc . . .

For $T_e \sim 200$ eV , $\beta << 1$ and so ions with charge state $< Z - 2$ can be neglected. Then in equations (1) and (2)

$$N_e = [\, (8 + 7\alpha)\, N_e .\, N(C^{6+}) \,]^{\frac{1}{2}}$$

where the product $N_e\, N(C^{6+})$ is measured from the intensity of the recombination continuum into C^{6+} and α from the ratio of C^{6+} continuum and C^{5+} continuum. The average density measured this way within a layer 50 microns in depth from the original target surface is

$$N_e \text{ (free-bound continua)} = 5.0\ (\pm\ 2.5) \times 10^{20} \text{cm}^{-3} \ .$$

The error in the above value is mainly due to uncertainty in the plasma volume V , and the emission time t . The above density has to be corrected for several systematic errors. For example, we have to take into account a correction for the population of CVI ions in excited states, since only electronic recombination into the ground state, has been measured. The partition functions may be derived from the tables of Drawin and Felenbok (1965). For our plasma density and temperatures we have

$$\sum_{n=1}^{(\psi/\Delta E)^{\frac{1}{2}}} N(C^{5+})_n \ / \ N(C^{5+})_{n=1} \simeq 5$$

ΔE is the reduction in the ionisation potential, ψ , due to the ions being immersed in the plasma, and is of the order of a few eV, in our case. Thus, taking into account the partition function for the CVI ion we have a revised estimate of $N_e \sim 8.0 \times 10^{20}$ cm^{-3} .

The ionisation potential depression is sufficiently small for us to ignore this correction in the calculations of the continua intensities (1) and (2). However there is an apparent shift of the continuum limit due to merging of the upper levels which are broadened by the Stark effect. The density may be derived directly, albeit less accurately, from the quantum number n_m associated with the last discrete line of the series according to the formula of Inglis and Teller (Griem 1964)

$$n_m^{z-1} = {}^1/_2 \,.\, Z^{3/5} \,.\, (a_o{}^3\, N_e)^{-2/15} \qquad \ldots(5)$$

where a_o is the Bohr radius. Within 50 micron from the surface, n_m is between 4 and 5, and

$$N_e \text{ (series-merging)} \sim 2.5 \times 10^{21} \text{ cm}^{-3} .$$

This corresponds with the absolute intensity measurements above. Further out from the target surface progressively higher members of the Lyman series are noted. The density evaluated using both techniques and the free electron temperature are plotted as a function of distance from the target in Figure 4, for an incident laser of $\sim 10^{12}$Watts/cm^2. The full lines are the predictions of the 'Medusa' 1-dimensional hydromagnetic code, described by Ashby and Christiansen (1973). Since the side-wise expansion time is of the same order as the laser pulse, a 1-D approximation, ie. expansion only along the target normal, is reasonable for the plasma dynamics. The significance of these results will be discussed in Section 10.

5. ELECTRON TEMPERATURE DEPENDENCE ON FLUX INTENSITY

The theoretical scaling law of the plasma temperature, T_e , against radiant flux intensity, ϕ , depends on the absorption mechanism and on the model chosen for the expansion hydrodynamics, see for example Floux (1971) and Krokhin (1972). Donaldson,Hutcheon and Key (1973) give a useful set of references for these theoretical models and report measurement of $T_e \propto \phi^{0.44}$ which is in agreement with inverse Bremsstrahlung absorption and 2-dimensional expansion.

Figure 5 shows the variation of peak temperature derived in Section 3, against peak flux intensity. A best fit to our results gives:

$$T_e(\text{eV}) = 1.4 \times 10^{-4} \, \phi^{(0.52 \pm 0.03)} \qquad \ldots(6)$$

A $\phi^{2/3}$ slope is also included in the figure for comparison, since it represents a limiting case where the deposition of the radiant energy is localised in a plane at the critical density, and the temperature is time-independent. In Figure 4 the full curves are calculated for deposition at the critical density of that fraction of the laser energy not absorbed by inverse - Bremsstrahlung.

There is good evidence, in this study, that local deposition of a significant fraction, ~ 30% , of the laser energy takes place within a few wavelengths at the critical density and that a 1-dimensional approximation is a reasonable description of the hydrodynamic expansion. It is apparent however that our exponent in the power law equation (5) falls between the value of $^{2}/_{3}$ expected from the time-independent model and the value of $^{4}/_{9}$ reported by Donaldson et al (1973). Our errors cannot accommodate either value. In the latter comparison, however, the difference may be explained by the approximation to planar dynamics in our case and to spherical dynamics in the case of Donaldson et al.

6. THE RELATIVE ION POPULATIONS IN THE ABSORPTION LAYER

The relative populations of the C^{6+} and C^{5+} ions are derived directly from the relative intensities of the respective free-bound continua according to equation (1). Figure 6 shows a plot of the experimental ratio for the relative ground level populations as a function of laser flux intensity.

In order to relate these population ratios to the heating time (section 9) it is necessary to choose an ionisation model, McWhirter (1965), which is appropriate to the plasma parameters in the absorption layer and to solve the time-dependent ionisation equations. An assumption basic to these models is that the electron energy distribution is Maxwellian, but this has already been justified, section 3. The steady-state, ground-level population ratios for a number of different models have been calculated and are plotted in Figure 6. Only the model based on the collisional radiative coefficients calculated by Bates, Kingston and McWhirter (1962) is appropriate to our case, however.

The conditions that there should be less than 10% departure in level m from local thermodynamic equilibrium (LTE) (McWhirter, 1965) is

$$N_e . N(m) . \chi(T_e, m, n') \gtrsim 10 . N(m) . A_{mn'} \qquad \ldots (7)$$

At the critical density, 10^{21} cm^{-3}, and over the range of temperature from 100 eV to 200 eV, the collisional limit, m_ℓ , is between principal quantum number 2 and 3. Levels $m \gtrsim 3$ are in collisional equilibrium with the

free electrons. Use of the coronal ionisation model but with an effective reduction of the ionisation potential to that of the $m_\ell = 3$ level is shown as a broken line in Figure 6 and is a reasonable approximation for the collisional radiative calculations.

Optical opacity causes an effective lowering of the spontaneous decay rate $A_{(m\,,\,n')}$ so that in equation (7), the RHS should be divided by $\bar{\tau}_o\ (m\ n')$, the optical depth. Optical opacity of the Lyman series has been studied for this plasma and is the subject of a separate publication, Galanti et al (1974). From that study, Lyman α has an optical depth of ~ 50 with that of higher members becoming progressively less; Lyman γ already has an optical depth $\tau_o\ (4,1) < 1$ due mainly to Stark broadening. The collisional radiative model of Bates et al (1962) in which the first resonance line is optically thick is therefore the most appropriate model and has been used in the comparison with the experimental results. The important point to note is that the experimental ratios of the ground level populations $N_g(C^{6+})/N_g(C^{5+})$ approach a value two orders of magnitude less than those calculated for the steady-state. The absolute population of the C^{6+}, C^{5+}, ions from equation (4), and of the electrons, are included in Table 1. The peak values should be scaled up by the same volume correction factor discussed in Section 11.

TABLE 1

Electron and Ion populations averaged over 50 microns at the target surface

Radiant Flux intensity: 5×10^{11} watts/cm^2. T_e=170 eV

$N_e = 8 \times 10^{20}$ cm^{-3}

$N\ (C^{6+}) = 2 \times 10^{19}$ cm^{-3}

$N\ (C^{5+}) = 2 \times 10^{20}$ cm^{-3} (ground level population multiplied by partition function)

$N\ (C^{4+})_g \sim 1 \times 10^{19}$ cm^{-3} → 1×10^{20} cm^{-3}

$N\ (C^{3+})_g \sim 5 \times 10^{16}$ cm^{-3} → 5×10^{17} cm^{-3}

7. INTERPRETATION OF SATELLITE INTENSITIES

Screened transitions giving rise to 'satellite' lines which lie on the long wavelength side of the He- and H-like resonance lines are prominent features of the soft X-ray emission spectrum from laser-produced plasmas, Peacock et al (1973). That these satellites are observed only in the intense continuum close to the target surface, can be confirmed by reference to the spatial variation of the satellite to the C VI, Lyman, series shown in Figure 2. We restrict our attention in this section, to satellites adjacent to the C V, $1s^2\ {}^1S_o$ - $1s2p\ {}^1P_1$, transition and make use of the fact that the separate multiplets at 41.34 Å , 41.37 Å and 41.55 Å, Figure 7, are resolved in wavelength and space. Following the general theoretical treatment outlined by Gabriel and Jordan (1971) and by Gabriel (1972) we can, from the intensities of the satellites, deduce the populating and depopulating rates from their upper levels.

Two possible mechanisms exist for populating the doubly-excited satellite levels, viz. dielectronic recombination from the He-like ion, Burgess (1965), or direct electron impact excitation from the ground level of the Li-like ion. In the optically-thin approximation the contribution from direct excitation yields an intensity ratio of the satellite, I_s' , to the allowed line, $1s^2\ {}^1So$ - $1s2p\ {}^1P_1$, which is given by

$$\frac{I_s'}{I} = \frac{N_{(Li)}}{N_{(He)}} \cdot \frac{1}{(1+\alpha)} \cdot \beta \frac{\bar{f}'}{f} \frac{A_r}{(A_a + \Sigma A_r)} \qquad \ldots(8)$$

where $N_{(Li)}$ and $N_{(He)}$ are the ground state level populations of Li- and He-like ions respectively. A_a and A_r are the transition probabilities for decay of the satellite level by auto-ionisation and by radiation respectively and the rest of the factors are as defined by Gabriel (1972). The $1s2p^2\ {}^2p^e$ terms at 41.37 Å , Figure 7, are metastable to auto-ionisation on account of parity and are therefore populated entirely by impact excitation from the Li-like ground level. Equation (8) may therefore be used directly to evaluate the

population ratio:

$$\frac{N_{Li}}{N_{He}} \quad \underline{ie} \quad \frac{N(C^{3+})}{N(C^{4+})} \quad .$$

The requirement for I to be optically thin can be circumvented by considering those optically thin satellites where dielectronic recombination populates their upper levels and contributes to an intensity, I_s . In this case, Gabriel (1972), the satellite to resonance line ratio is

$$\frac{I_s}{I} = \frac{0.01104}{(1+\alpha)} \quad \frac{E_o}{T} \exp\left[(E_o - E_s)/kT\right] \frac{g_s A_r A_a}{A_a + \Sigma A_r} \qquad \ldots(9)$$

where $(E_o - E_s)$ is the difference between the energy of the $1s2p\ ^1P_1$ level and of the satellite level above the ground state of the He-like ion. The other symbols are as defined by Gabriel (1972). Expression (9) applies to the multiplets of $1s2p^2\ ^2D^e$ and $1s2p2s\ ^2P^o$ which theoretically should have relative strengths of 1:0.95, (Bhalla and Gabriel, private communication). This is in good agreement with the observed ratio of 1:1, Figure 6, confirming a dielectric recombination mechanism for populating these levels. Peacock et al (1973) have noted that while the $1s2p^2\ ^2D^e$ multiplet becomes relatively more intense for ions with charge states much higher than carbon in laser-produced plasmas, a choice of either multiplet makes little difference in the present analysis.

We define the intensity of the $1s\ 2p^2\ ^2P^e$ multiplet by I_{s_1} and of the $1s\ 2p(^1P)2s\ ^2P^0$ multiplet by I_{s_2} ; then

$$\frac{I_{s_1}}{I_{s_2}} = \frac{\left(\frac{I_{s_1}}{I} \cdot F(^{Te}/_{T_m}) + \frac{I_{s_1}'}{I} \cdot F'(^{Te}/_{T_m})\right)}{\left(\frac{I_{s_2}}{I} \cdot F(^{Te}/_{T_m}) + \frac{I_{s_2}'}{I} \cdot F'(^{Te}/_{T_m})\right)} \qquad \ldots(10)$$

where the first term within the brackets on the RHS describes the dielectronic contribution and the second term the impact-excitation contribution to the total satellite intensity. The functions $F(^{Te}/_{T_m})$, $F'(^{Te}/_{T_m})$ are scaling factors dependent on the electron temperature, T_e , normalised to the temperature, T_m , at which the He-like ion has a maximum relative population in the steady state.

At T_e = 170 eV, typical of the spectrum in Figure 6, $F(^{Te}/_{T_m}) = 0.24$. Inserting theoretical values for the intensity ratios for the satellite to allowed line ratios, and correcting the ground level population of the C^{3+} ions (x0.73) for the proportion in the $1s^2 2p$ states, we can equate the theoretical ratio on the RHS of (10) to the observed ratio, viz

$$\frac{I_{s_1}}{I_{s_2}} = 0.95 = \frac{.0002 \times 0.24 + .0005\ F'(^{Te}/_{T_{m_1}})\ 0.73}{.0048 \times 0.24 + 0}$$

ie. $F'(^{Te}/_{T_m}) = 2.86$ yielding an equivalent steady-state electron temperature T_e' of 0.5×10^6 K, which is characteristic of the actual ground state population ratio for $N(C^{3+}) / N(C^{4+})$. Since we have quite generally, at temperature T_m ,

$$\frac{N_{(Li-)}}{N_{(He-)}} = 1.5 \times 10^{-4} (Z-3)^2 \qquad \ldots(11)$$

where Z is the nuclear charge then;

$$\frac{N(C^{3+})}{N(C^{4+})} = 1.5 \times 10^{-4} . (3)^2 . 2.86 = 3.9 \times 10^{-3}.$$

The derivation of this ratio, which refers to the ground state populations, is independent of the ionisation model and of optical opacity considerations,

8. INTERCOMBINATION LINE INTENSITY

In the low density limit where a coronal model is valid (McWhirter 1965) the relative intensities of the allowed $1s^2\ ^1S_o - 1s2p\ ^1P_1$, I, and of the intercombination line $1s^2\ ^1S_o - 1s\ 2p\ ^3P_1$, I_{13}, are determined only by the respective excitation rates from the ground state for a given ion. Where the inter-system collision rate, X_{23} , and the spontaneous decay rate of the triplet, A_{31} , are of the same order, the intercombination to allowed line intensity ratio can have a linear dependence on the electron density, Kunze, Gabriel and Griem(1968).

In the very high density limit however, when $n_e X_{23} \gg A_{21}$, where A_{21} is the allowed line spontaneous decay rate, then all of the $n = 2$ states are statistically populated and the relative intensities are given by

$$\frac{I_{13}}{I\ (thin)} = \frac{A_{31}}{A_{21}} = 3 \times 10^{-5} \text{ (high density limit)} \qquad \ldots(12)$$

The A values are taken from Elton (1967), and I(thin) is to be taken as the allowed line intensity in the optically thin approximation. The triplet-singlet collision rates, Gabriel and Jordan (1971), are given by

$$X_{23} = \frac{8.36 \times 10^{-8}}{Z\ (k\ T_e)} \quad cm^3\ sec^{-1} \ ,$$

where $Z = 5$ for $C\overline{V}$.

For the parameters in the absorption layer, $N_e \sim 10^{21}\ cm^{-3}$ and $T_e \sim 170$ eV, then

$$N_e\ X_{23} \lesssim A_{21} \quad \text{and} \quad N_e X_{2\,n\to\infty} \sim A_{21} = 4 \times 10^{11}\ sec^{-1} .$$

In the case of an optically thick resonance line the transition probability should be divided by the optical depth, $\tau_o(\nu)$, section 9, so that the high density limit should be a reasonable approximation for $C\overline{V}$ in our plasma. From Figure 7 it is readily deduced that

$$\frac{I_{31}}{I} \text{ (experiment)} = 6.03 \times 10^{-2} \qquad \ldots(13)$$

taking into account the emulsion response. Comparing values derived in (13) and (12), the allowed line intensity, based on the observed strength of the inter-combination line, is only 5×10^{-4} of its optically thin value. It is clear therefore, that the intensity profile of the allowed line is determined by optical opacity. The calculation of the optical depth based on the satellite intensities, section 9, is likely to be more reliable because the intensity of the relatively weak intercombination line feature may be partly due to weak satellites eg $1s^2 2p\ ^2P^o - 1s2p^2\ ^2S$, unmarked in Figure 7. Also local thermodynamic equil-ibrium is an extreme limit which can only be approximately valid for the n=2 state.

9. OPTICAL OPACITY

Since the optically thin intensity of the allowed line intensity, $I_{(thin)} = \int^{s} N(CV, 1s2p\,^1P_1) \cdot \frac{h\nu}{4\pi} \cdot A_{21} \cdot ds$, where the integration $\int^{ds}$ is taken over the line sight, can be derived directly in units of I_{s_2} from equation (9), comparison with the experimental value gives some information on its optical opacity.

From equation (9) we have

$$\frac{I_{s_2}}{I\ (thin)} = .0048\ F(T_e/T_m) = 1.15 \times 10^{-3}$$

But from Figure 7 taking into account the emulsion response $\frac{I_{s_2}}{I}$ (experiment) $= \frac{1}{6}$

$$\text{ie.} \quad I\ (\text{experiment}) = 6.9 \times 10^{-3}\ I(\text{thin}) \qquad \ldots\ (14)$$

The allowed line intensity, taking into account optical opacity and collisional de-excitation of the n = 2 states, can be expressed as

$$I = \frac{N_1(C^{4+})\ X_{12} A_{21}}{(\sum_{p=3}^{\infty} n_e X_{2p} + A_{21})} \cdot \frac{h\nu}{4\pi} \cdot g(\tau_o) \qquad \ldots(15)$$

where $g(\tau_o) = [\ \tau_o(\pi\ \ln\tau_o^{\frac{1}{2}})]^{-1}$ is the escape factor after Holstein (1947), τ_o is the optical depth at the line centre and X_{2p} $cm^3 sec^{-1}$ is the collisional rate coefficient. Depending on the total collisional de-excitation rates, the factor in (14) predicts an optical depth of between 5 and 50. It is thus possible to derive directly an order of magnitude for $N(C^{4+})$, and hence from section 7, for $N(C^{3+})$, from the value of τ_o. These ion populations are inserted in Table 1.

10. IONISATION TIME IN THE ABSORPTION LAYER

Since a steady-state ion population is not achieved, Figure 6, the time-dependent equation for completely stripped carbon ions can be written

$$\frac{dN(C^{6+})}{dt} = N_e\, N(C^{5+})\, S_{cr}(C^{5+}) - N_e\, N(C^{6+})\alpha_{cr}(C^{6+}) \quad \text{---- (a)}$$
$$N(C^{6+}) + N(C^{5+}) \simeq \text{const.} \quad \text{---- (b)} \qquad \ldots(16)$$

where S_{cr} and α_{cr} are the radiative-collision rate coefficients, Bates et al (1962). As the ionising time from $N(C^{5+})$ to $N(C^{6+})$, $(S_{cr})^{-1}$ is, in our range of temperature, more than 5 times greater than the ionisation from $N(C^{4+})$ to $N(C^{5+})$ then the solution of (16) gives approximately the total heating time, viz.,

$$\frac{N(C^{5+})}{N(C^{6+})} - \frac{\alpha_{cr}(C^{6+})}{S_{cr}(C^{5+})} = \left(\frac{N(C^{5+})}{N(C^{6+})} + 1 \right) e^{-N_e(\alpha + S)\tau} \qquad \ldots(17)$$

Identifying the first factor on the LHS as the experimental ratio R, and the second factor as the steady state value R_s, then

$$R - R_s = (R + 1)\, e^{-\tau/\tau_s} \qquad \ldots(18)$$

where τ_s, the time to reach a steady state, is given by

$$N_e \tau_s = \frac{1}{[\alpha(C^{6+}) + S(C^{5+})]} \qquad \ldots(19)$$

Using the experimental and steady-state population ratios, Figure 6, in expression (18) we derive $N_e \tau$, the product of the electron density and the heating time.

The variation of $N_e\tau$ with laser flux intensity is of some importance in any consideration of the ionising efficiency of the laser plasma. In Figure 8 we choose to plot $N_e \tau$ against the plasma temperature which is itself uniquely defined by the flux intensity.

The collisional radiative curve is most applicable, though a derivation assuming the coronal coefficients as has been used by other authors, is inserted for comparison.

The first essential point is that the heating time for the ions is exceedingly short; $N_e \tau$ is in the range 10^{10} to $10^{9} cm^{-3}$ sec so that τ, the ionisation time is of the order of 10^{-11} to 10^{-12}secs. This is at least one order of magnitude less than the ionisation time derived from model calculations by Donaldson et al (1973), Combant and Tonon (1973).

Secondly, the value of $N_e \tau$ increases monotonically with temperature so that as the flux intensity increases over the range 10^{11} to 2×10^{12} watts/cm^2 the plasma becomes progressively more efficient at producing highly ionised species.

11. DISCUSSION OF RESULTS

From the $N_e \tau$ values derived above the depth of the ionising layer, ℓ_i, may be deduced by equating the time to reach the observed ionisation state, τ with ℓ_i / v_s, where v_s is the ion escape velocity. A reasonable assumption is that the escape velocity is of the same order as the ion sound speed, v_z, ie

$$v_s = v_z = [(k T_e + Zk T_i)/M(Z)]^{\frac{1}{2}} .$$

The confinement time of the C^{6+} ions (10^{-11}secs to 10^{-12}secs) is shorter than the thermalisation time (25×10^{-12}secs) between the electrons and ions. Energy relaxation between the particle species is therefore incomplete and $T_i < T_e$. Taking $T_e = 220$ eV, Figure 4, and assuming $T_i = T_e/2$, as an approximate value, then $v_z \simeq 3.2 \times 10^{6} cm\ sec^{-1}$. Since, at an electron temperature of 220 eV, from Figure 8 $n \tau = 10^{10} cm^{-3}$ sec, then $\ell_i \simeq 0.3$ microns. For escape velocities higher than v_z, the ionisation layer is proportionately longer.

We can illustrate that this very narrow ionisation layer is not unreasonable by evaluating the rate of ionisation in each element of the plasma depth measured along the target normal. Consider an ion escaping from near the solid surface towards the incoming laser beam, then the change of ionisation per unit

depth , dx at x is

$$\delta N_z(x) \propto N_e\, N_z \langle \sigma v \rangle^i\, \delta x / v_s \qquad \ldots (20)$$

From particle flux conservation in 1-dimension

$$\nabla (N_e\, v_e) = 0 \quad \text{ie} \quad v_e(x) \propto \frac{1}{N_e(x)} \ .$$

Also from Figure 4 and extrapolating linearly from the experimental temperature and density values, we have the approximate relations:

$$T_e \propto (x)^{-\frac{1}{2}} \ ; \quad N_e \propto (x)^{-1} \ .$$

Inserting these scaling factors in equation (20) and using an appropriate expression for the ionisation rate $\langle \sigma v \rangle^i$, we have,

$$\delta\, N_z(x) \propto N_e^{\,3} .\ N_e^{\,1/8} .\ e^{-\{\text{Const.}\psi.x^{\frac{1}{2}}\}} .\ \delta x \qquad \ldots (21)$$

For $\underline{\text{CVI}}$, the ionisation potential, ψ , is 490 eV. From equation (21), and inserting the experimental parameters, it is readily deduced that:

$$\delta N_z(x_o) \ = \ 176 \times \delta N_z(x_o + 30\mu) \ = \ 22{,}000 \times \delta N_z(x_o + 100\mu),$$

where x_o is the plasma depth corresponding to the highest extrapolated value of the electron temperature profile. Ionisation is evidently confined to a very narrow layer, $\leqslant$ 1 micron in depth in the highest pressure region, where the mean free path of the ions between ionising collisions,

$$\text{ie} \quad \lambda^i_{ei} = v_z \{N_e \langle \sigma v \rangle^i\}^{-1} \simeq 0.05 \text{ microns.}$$

In view of the probability that the spatial extent of the high temperature continuum emitting region is considerably less than that subtended by the spectrograph optics (in section 2), we have to admit to a re-evaluation of this emission layer in order to arrive at a value for the <u>peak</u> electron density. The average densities in Table 1 have to be scaled up by a factor $\left\{0.0050/\ell_e\right\}^{\frac{1}{2}}$, where ℓ_e is the actual depth of the layer emitting the Lyman continuum. Independent methods for measuring the density close to the target (Galanti, Peacock et al (1974),

using Stark broadening of H_α and L_γ and using also the intensity ratios of $L\beta/L_\alpha$ of CVI, place the peak value at between 2 x and 4 x $10^{21}cm^{-3}$, ie slightly above the critical density for reflection. This would correspond to a scale length ℓ_e, for the Lyman continuum emission of the order of 3 microns. Since this revised peak density has now to be inserted in the $N_e \tau$ product; a corrected value for the ionisation scale length, ℓ_i, $\simeq 10^{-5}$ cm. This value is a lower limit since it is difficult to conceive of an escape velocity less than the ion sound speed. The ionisation could possibly have a scale length equal to the emission depth ($\sim$ 3 microns) only provided that the escape velocity of the ions is increased to $\sim 10^8 cm\ sec^{-1}$, which seems an improbably high value.

It has been brought to our attention* that any attempt to equate simultaneously the extent of the emission region, ℓ_e, with the ionisation scale length ℓ_i, derived from $Ne.\ell_i/v_z$, where v_z is the ion sound speed, leads to an unrealistically high density and conversely an improbably shallow ionisation layer. There is however, no a priori reason to suppose that these two scale lengths should be the same.

Since the density and temperature profiles $T_e(x)$, $N_e(x)$ have been measured it is pertinent to calculate the spatial variation of the radiant energy intensity in the plasma, viz

$$\phi(x) = \phi_o\, e^{-\int_{x=\infty}^{x} \kappa[N_e(x),\, T_e(x)]\,dx}$$

where ϕ_o is the laser intensity at $x = \infty$, and $\kappa[N_e(x), T_e(x)]$ is the resistive absorption coefficient given, for example, by Dawson (1964).

Figure 9 illustrates a calculation of the radiant energy profile which includes a correction for the breakdown of the geometrical optics approximation which occurs over the last few microns close to the critical surface. Assuming a linear variation of the dielectric permittivity over the last few

* The inconsistency in equating ℓ_e and ℓ_i has been brought to our attention by the referee.

microns it is possible to calculate an exact solution in the boundary layer according to Ginzburg (1964). This gives a correction of about 50% to the absorbed flux in this region , viz,

$$\phi_{absorbed} = \phi_{inc}\left(1 - \exp\left\{-2\left[\int \kappa(x)\,dx + \frac{2\pi}{\lambda}\,\frac{\sqrt{2}}{3}\,B^{3/2}\Big/ d\varepsilon/dx\right]\right\}\right)$$

where B is the reduced electron-ion collision frequency. A theoretical treatment of the variation of the incident and reflected power for very similar irradiation conditions has been derived by Mulser et al (1973) and their calculations compare well with our experimental results, showing that resistive absorption is the main operative absorption process. Figure 9 shows that an appreciable fraction, about 30%,of the incident energy is absorbed within 10μm from the reflection point. Only a few per cent of the light should be reflected, and this agrees in order of magnitude, with the observed values for the reflected laser energy in our experiment. We have considered the plasma heating at densities above the critical density. Electron heat conduction into the target will alter the temperature profile according to

$$\frac{\partial kT_e}{\partial \tau} = \frac{K_H}{n_e}\,\frac{\partial^2 T_e}{\partial x^2} \quad , \qquad \ldots (22)$$

where K_H is the electron heat conduction coefficient, Spitzer (1956). The temperature profile is set up extremely rapidly, $\sim 10^{-11}$ secs, and retains a steep front during the laser pulse; see the results of the numerical code, figure 4. A characteristic propagation length ℓ_H is

$$\ell_H = \left(\frac{K_H}{kn_e}\,\tau\right)^{\frac{1}{2}} \qquad \ldots (23)$$

Identifying τ with the confinement time for the ions (ie the hydrodynamic expansion time of the plasma at the critical density) we derive a heat penetration length of 0.5 μm at solid density and a factor of ten times this value at the critical density. Plasma heating at densities just above the critical value can

therefore be accounted for and indeed there is evidence for it in the theoretical and experimental profiles in Figure 4. Radiation transport from the core of the optically-thick Lyman lines of C^{5+} is also a possibility, Galanti, Peacock et al (1974).

While resistive absorption of the incident light coupled to heat propagation into the target can account for the deposition of a substantial fraction, $\sim 30\%$, of the radiant energy within a shallow plasma layer, of the order of 10 microns; the depth of the ionisation layer has been shown above to be even smaller, less than 1 micron, if the escape velocity is the ion sound speed. It is possible that collisionless processes, such as resonance absorption, Vinogradov and Pustovalov (1971), Friedberg et al (1972), play a more important role in the critical-density layer itself than resistive absorption. In resonance absorption the transverse EM wave is transformed into Langmuir waves which are propogated parallel to the density gradient. An important parameter in this case is the scalelength for the density inhomogeneity

$$a = N_{crit} / \left(\partial N / \partial x\right)_{x=0}$$

where $x = 0$ is the location of the critical density along the target normal. Using our results (Figure 4), $a \sim 50$ microns. The damping length for the waves is then

$$\ell' \sim a(\nu/\omega) ,$$

where ν sec^{-1} is the collision frequency and ω is the angular frequency of the incident laser beam. For our experimental conditions $\ell' \sim 1$ μm, in close agreement with the calculated depth of the C^{6+} emission layer. Assuming that a fraction of the incident light energy, ϕ_A of the order of $0.3\phi_o$, is absorbed entirely at the critical density, then by energy balance we have

$$\overline{kT}_e \sim \phi_A / N_{ec} v_z$$

ie.
$$\overline{kT}_e \text{ (eV)} = 6 \times 10^{-6} \phi_A^{2/3} \quad (\phi_A \text{ in watts/cm}^2) \qquad \ldots (24)$$

Although the functional dependence on the absorbed flux (22) is not exactly the same as the observed temperature dependence on ϕ_o , equation (6), the relation (22) gives fair agreement with the observed results, figure 5. Further work is required to establish with certainty the existence of non-linear absorption over the range of incident flux intensity studied here. It is known that these non-linear processes become important at considerably higher light intensities. The efficiency of resonance absorption, Mueller (1973), depends critically on the angle of incidence and plane of polarisation of the light beam but these factors have not been investigated here.

A basic assumption in the comparison of our results with models of the light absorption and plasma dynamics has been that the density and temperature gradients are stationary in time during the laser pulse. This can be justified by the short heating time of the plasma relative to the laser pulse duration. Operation of the 1-dimensional Medusa code, Ashby and Christiansen (1973), in which the radiant energy not absorbed by resistive absorption in the incoming beam is dumped into the critical density layer, shows that the density evolves to an almost constant profile during the laser pulse. The critical density is maintained within 50 microns of the target surface over our range of flux intensity and follows closely the time-averaged experimental results, Figure 4. Lack of time-resolution in our study is therefore no severe handicap to the analyses. It is of interest to note that while the temperature in the region of the critical density is also correctly predicted by the Medusa code our results show a considerably steeper fall-off outwards from the target surface, Figure 4. This could be due to radiation cooling which is not accounted for in the present code format.

12. SUMMARY AND CONCLUSIONS

Quantitative spectroscopic measurements of the soft X-ray emission from the plasma produced close to the surface of laser-irradiated polyethylene target has been used to derive space-resolved values for the temperature and

density profiles. Up to the maximum light intensity studied here, 2×10^{12}watts/cm^2 , the electron velocity distribution is Maxwellian and shows no distortion due to non-linear light absorption.

The maximum temperature and kinematic pressure are located where the density just exceeds 10^{21} cm^{-3} ie where the light frequency and the plasma frequency are equal. The population of the carbon ions at the location of the critical density is interpreted on a transient ionisation model in which optical opacity of the lower bound states is important. From this model an ionisation time is derived. Making the assumption that the escape velocity from the ionisation layer is at the least of the order of the ion sound velocity then a scale length for ionisation is deduced which has a value of the order of one tenth of the wavelength (in vacuo) of the incident laser light. Classical resistive absorption and heat conduction would predict a somewhat wider zone of high pressure plasma, of the order of a few microns, from which the C^{6+} Lyman continuum is emitted.

It has been observed that both the electron temperature and the ionisation time for the ions increase with increasing radiant intensity at the target surface. Both these factors contribute to higher efficiency in producing highly-stripped species.

Qualitative confirmation of the efficiency of laser-produced plasma in producing highly-stripped ion stages has been domonstrated recently by the observation of H-like Mg $\overline{\text{XIII}}$ (Peacock et al, 1973) and Li-like V $\overline{\overline{\text{XXI}}}$ (Fawcett et al, 1974) using the same laser but at higher flux intensities $\sim 10^{13}$watts/cm^2. At a level of $\sim 10^{15}$watts cm^{-2} H-like T_i $\overline{\text{XXII}}$ has been observed (G McColl, Los Alamos Scientific Laboratory - private communication 1975). At these higher intensities light absorption is expected to be entirely be means of collisionless processes and heat conduction will become an important factor in the density and temperature profiles. It is inadvisable to extrapolate the

present scaling laws to considerably higher intensities but this will form part of our future studies.

ACKNOWLEDGEMENTS

The authors would like to record their appreciation to A H Jones for improvements to the laser system. Discussions with B A Norton on partition functions and the optical opacity of the Lyman series, and with A H Gabriel on the satellite line intensities, have helped our understanding of these problems. The help of D E T F Ashby and J P Christiansen with the numerical code and with discussions on the physics of the light-plasma interaction is greatly appreciated.

REFERENCES

1. Ashby DETF and Christiansen J P (1973), Proc. 6th Europ.Conf. on Controlled Fusion and Plasma Physics, vol 1, pp 431-434, published by Joint Institute for Nuclear Research, Moscow.

2. Bates D R, Kingston A E and McWhirter R W P (1962), Proc.Roy.Soc. A 270, pp 155-167; Plasma Physics and Controlled Nuclear Fusion Research, IAEA Vienna, pp 297-312.

3. Bobin J L (1971), Phys.Fluids, 14, 11, pp 2341-2354.

4. Burgess A (1965), Astroph. J. 141, pp 1588-1590.

5. Caruso A and Gratton R (1968), Plasma Physics, 10, pp 867-877.

6. Christiansen J P, Ashby D E T F and Roberts K V (1974), submitted for publication in Computer Physics Communications.

7. Colombant D, and Tonon G F (1973), J.Appl.Phys. 44, No 8, pp 3524-3537.

8. Drawin H W and Felenbok P (1965), Data for Plasmas in Local Thermodynamic Equilibrium, published by Gauthier-Villar, Paris.

9. Dawson J M (1964), Phys.Fluids, 7 , pp 981-987.

10. Donaldson T P, Hutcheon R J and Key M H (1973), J.Phys. B, vol 6, pp 1525-1544.

11. Elton R (1967), Astrophys. J. 148, pp 573-578.

12. Fawcett B C, Galanti M, Peacock N J (1974), J.Phys. B. 7, No 10 pp 1149-1153.

13. Fawcett B C, Galanti M, Peacock N J (1974), J.Phys. B, 7, No 4, L 106-107.

14. Floux F (1971), Nuclear Fusion, 11, pp 635-647.

15. Friedberg J P et al (1972), Phys.Rev.Letters, 28, No 13, pp 795-799.

16. Gabriel A H and Jordan C (1971), Case Studies in Atomic Collision Physics, vol II, Chapter 4, Eds. McDaniel and McDowell, North Holland Publishing Co.

17. Gabriel A H (1972), Mon.Not.Roy.Ast.Soc. 160, pp 99-119.

18. Galanti M, Peacock N J, Norton B A, Puric J (1974), Proc.Int.Conf. on Plasma Physics and Controlled Thermonuclear Fusion, paper CN-33/F3-4 Tokyo Proc. to be published by IAEA Vienna 1975.

19. Ginzburg V L (1964), Propagation of Electromagnetic Waves in Plasmas, Chapter IV, North Holland Publishing Company, Amsterdam.

20. Griem H R (1964), Plasma Spectroscopy, McGraw-Hill, New York.

21. Hobby M G and Peacock N J (1973), J.Phys. E, 6, pp 854-857.

22. Holstein T (1947), Phys.Rev. 72, pp 1212-1233.

23. Irons F E and Peacock N J (1973), J.Phys. E, 6, pp 857-862.

24. Irons F E and Peacock N J (1974) submitted to J.Phys. B.

25. Kaw P and Dawson J (1969), Phys.Fluids, 12, pp 2586-2591.

26. Kunze H J, Gabriel A H and Griem H R (1968), Phys.Rev. 165, pp 267-276.

27. Krokhin O N (1971), Physics of High Energy Density: 'Enrico Fermi' School of Physics, course 48, pp 278-305, Academic Press, New York.

28. Kruer W L and Dawson J M (1972), Laser Interaction and Related Plasma Phenomena, vol 2, pp 317-338, Editors - Schwarz and Hora, Plenum Press, New York.

29. McWhirter R W P (1965), Plasma Diagnostic Techniques, New York, Academic Press, Chapter 5.

30. Mueller MM (1973), Phys.Rev. Letters, 30, No 13, pp 582-585.

31. Mulser P, Sigel R and Witkowski S (1973), Physics Letters (review section) 6C, 3, pp 187-239.

32. Nuckolls J, Wood L, Thiessen A and Zimmerman G (1972), Nature, 239, pp 139-142.

33. Peacock N J and Pease R S (1964), Brit.J.Appl.Phys. (J Phys. D), 2, pp 1705-1715.

34. Peacock N J, Hobby M G and Galanti M (1973), J.Phys. B, 6, pp 298-304.

35. Speer R J (1972), Atoms and Molecules in Astrophysics, Academic Press, New York, pp 285-310; see also (1970) Adv. X-Ray Analysis, 15, 382.

36. Spitzer L (1956), Physics of Ionised Gases, Interscience Publishers Inc., New York.

37. Stratton T (1965), Plasma Diagnostic Techniques, chapter 8, Academic Press, New York.

38. Vinogradov A V and Pustelov V V (1971) Zh ETF Pis.Red 13, No 6, pp 317-320.

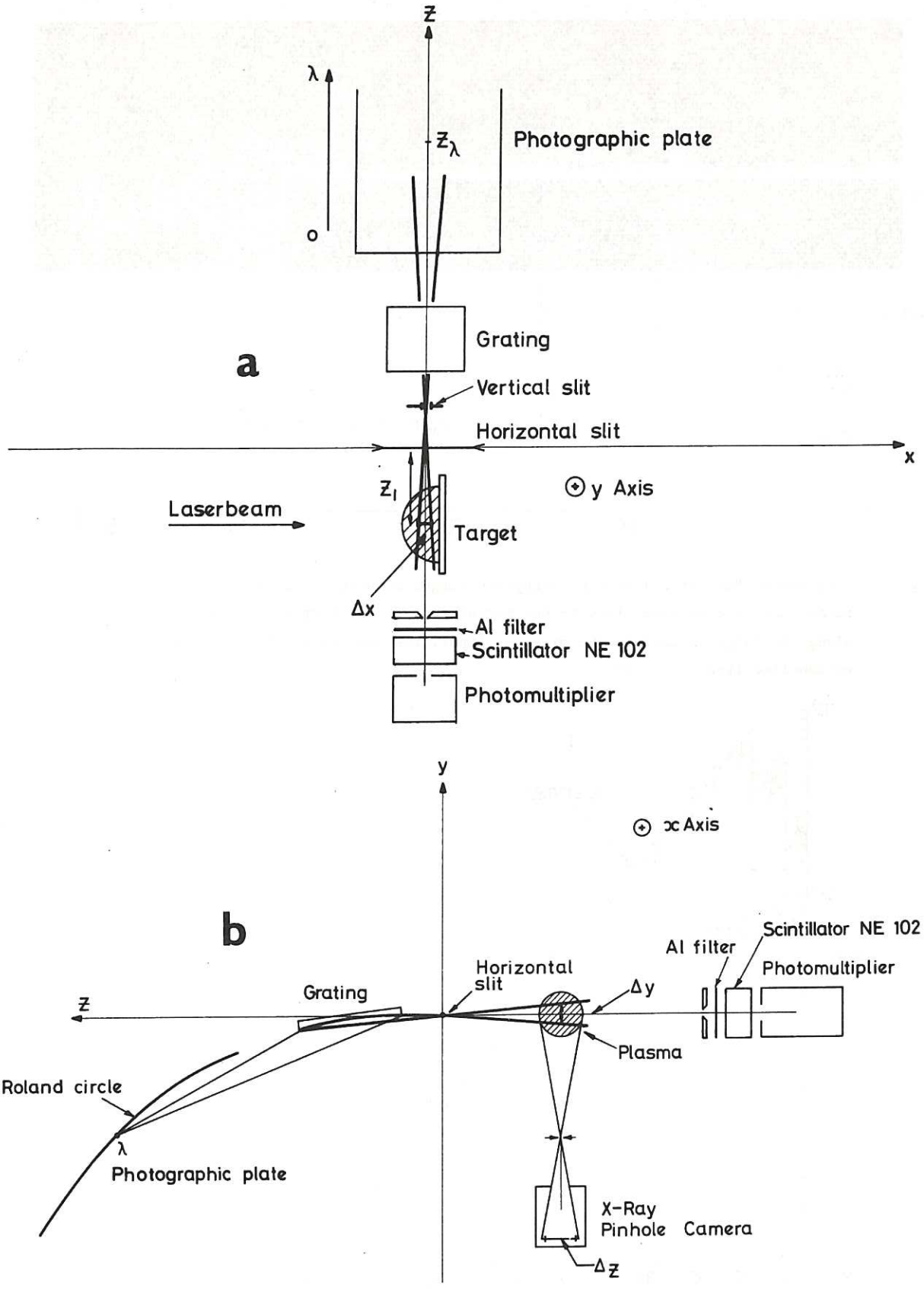

Fig 1. Schematic diagrams (a) and (b) of grazing-incidence spectrograph and associated apparatus for space-resolved X-ray measurements.

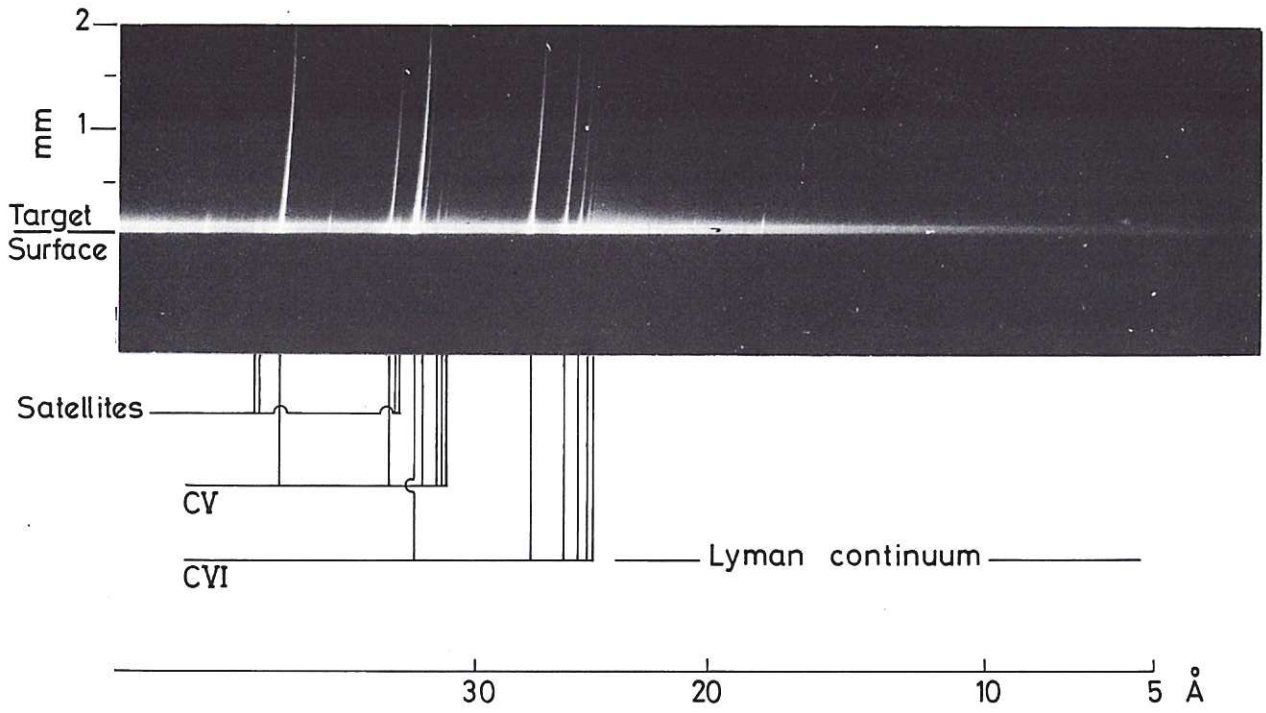

Fig 2. Spectrum of laser-irradiated polyethylene target showing the intense recombination continuum close to the target surface. The space-resolution along the target normal is 100 microns (impurities are responsible for the un-labelled line features).

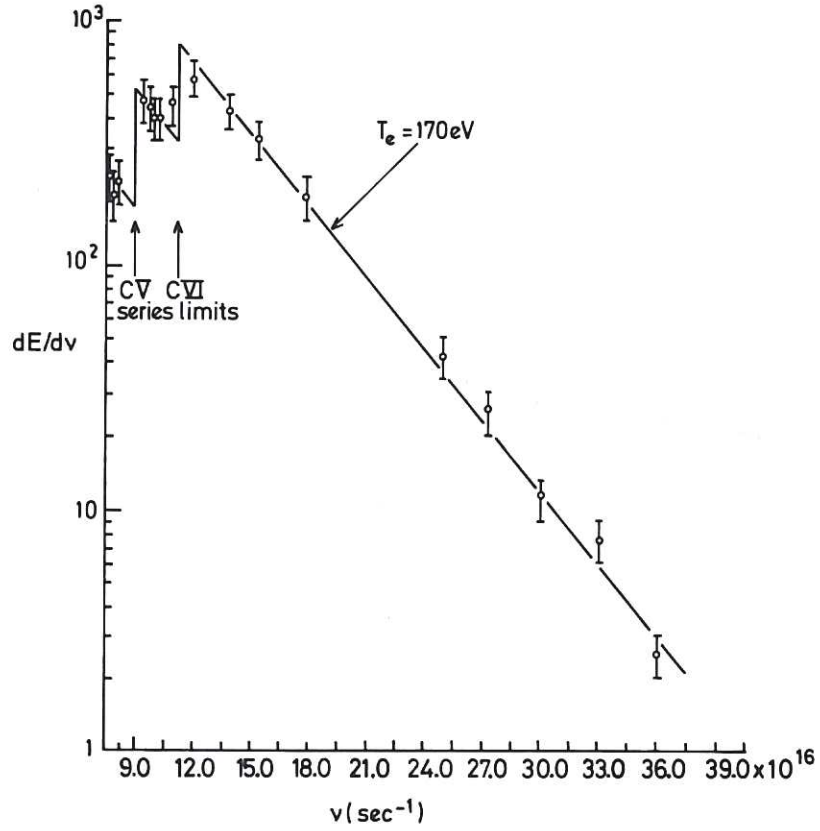

Fig 3. Photon energy distribution from the Lyman continuum emitted at a polyethylene surface irradiated by 1.06 micron laser beam with a flux intensity of 5×10^{11} watts cm^{-2} .

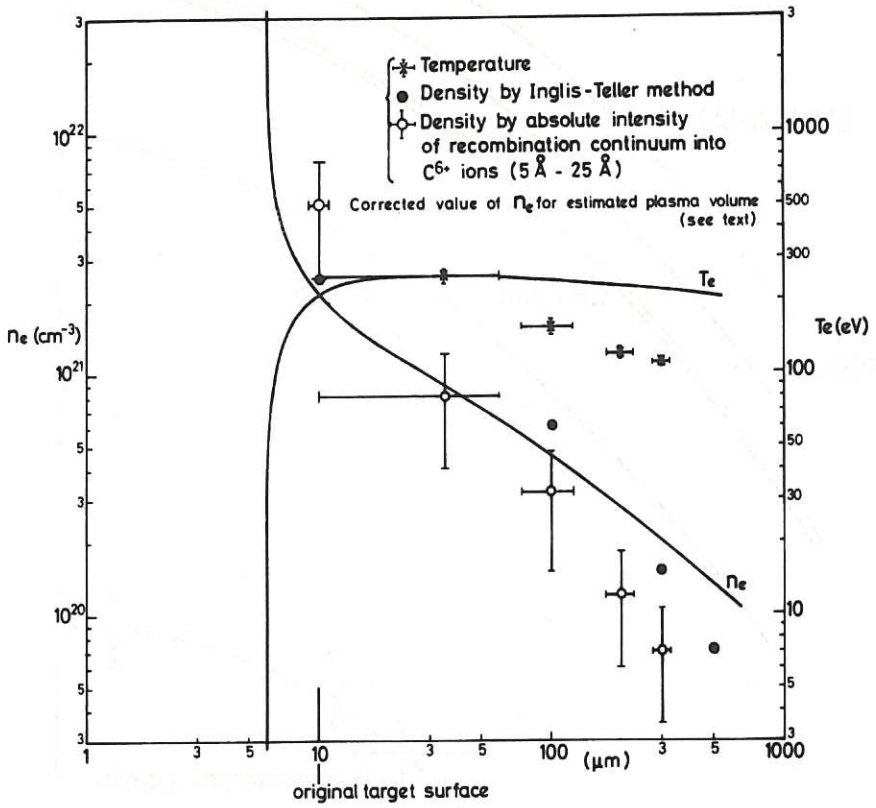

Fig 4. Predicted, time-averaged, density and temperature profiles along the normal to a polyethylene surface using the 1-Dimensional (Medusa) numerical code. The peak N_D laser power density is 10^{12} watts cm^{-2} in a 4.5 nsec long pulse, The experimental results for the same irradiation conditions are deduced from the spectroscopic data (see text) and are shown for comparison with the theoretical model profiles.

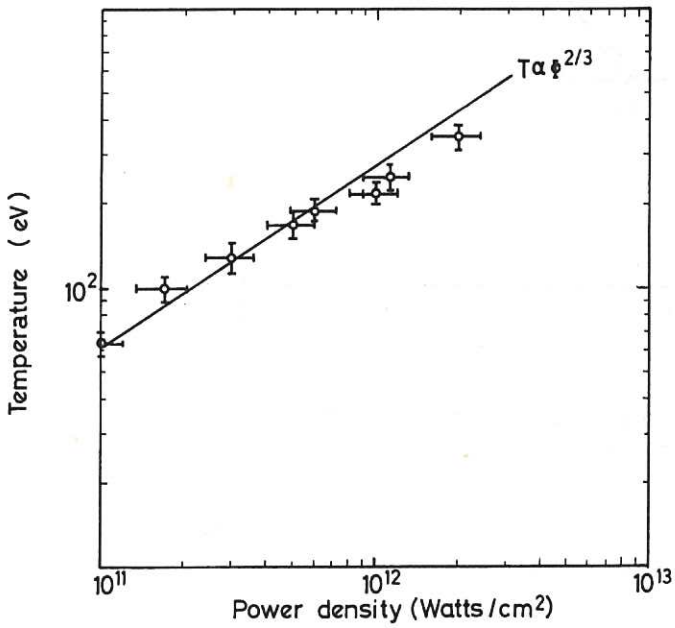

Fig 5. Plasma temperature (deduced from the Lyman continuum) versus laser power density at the surface of a solid polyethylene target.

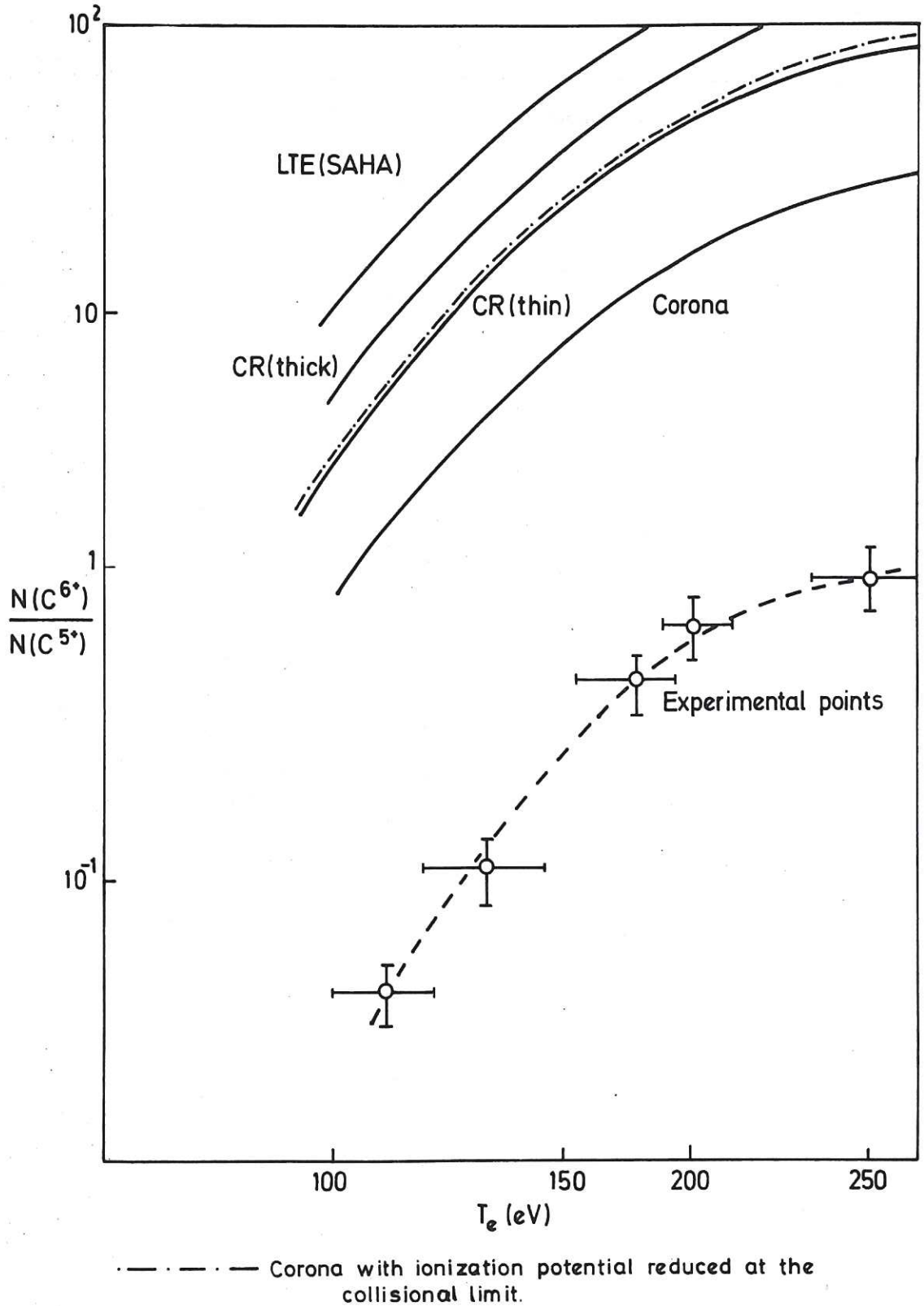

Fig 6. Theoretical prediction of the relative ion population of C^{5+} and C^{6+}, in the critical density region of the plasma. The calculations are based on a steady-state model. The ground state experimental ion population ratios are also shown.

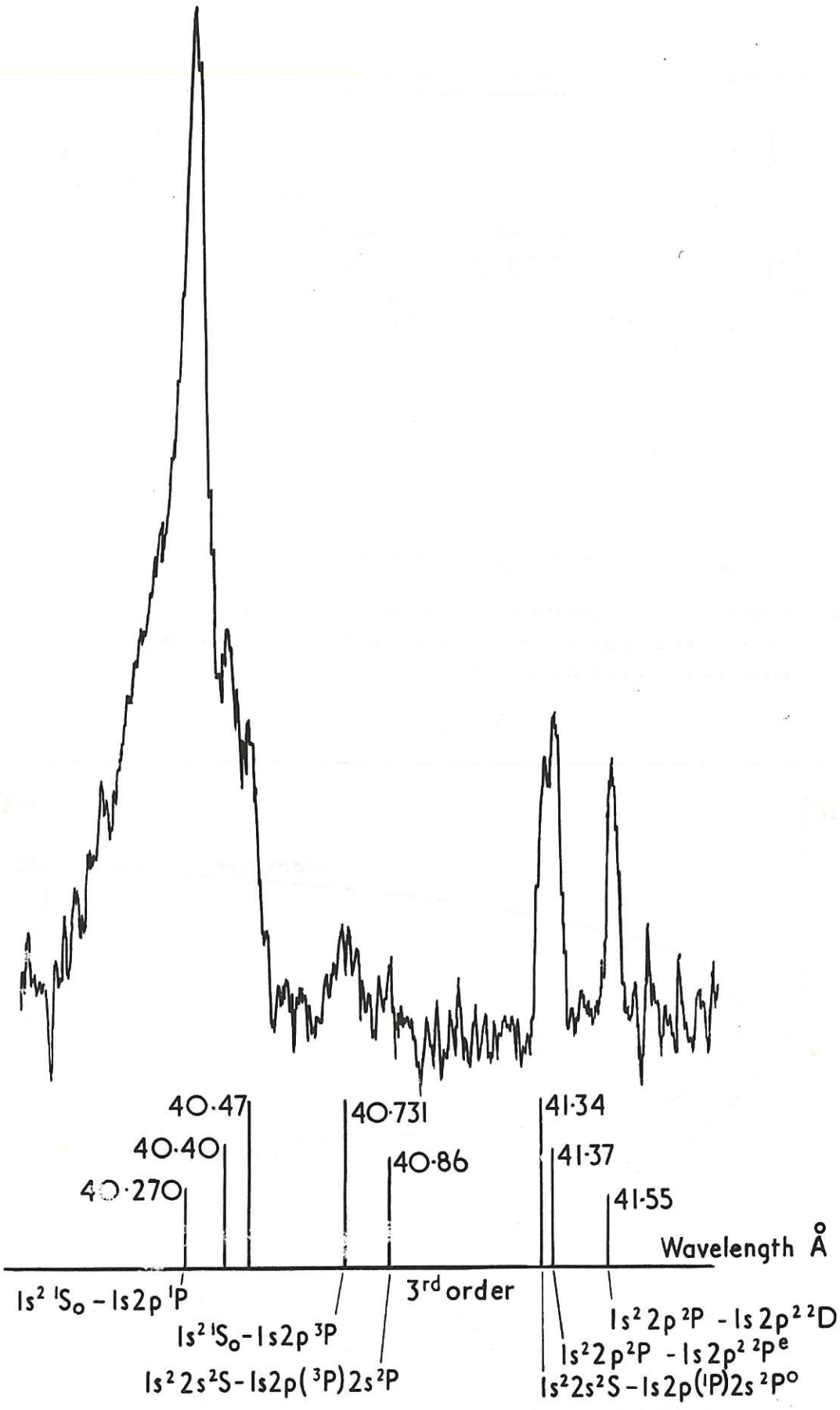

Fig 7. Part of the spectrum of a polyethylene plasma showing the CV, allowed and intercombination lines and the associated satellites. Power density on the polyethylene surface is 5×10^{11} watts cm^{-2} with an associated plasma temperature of 170 eV.

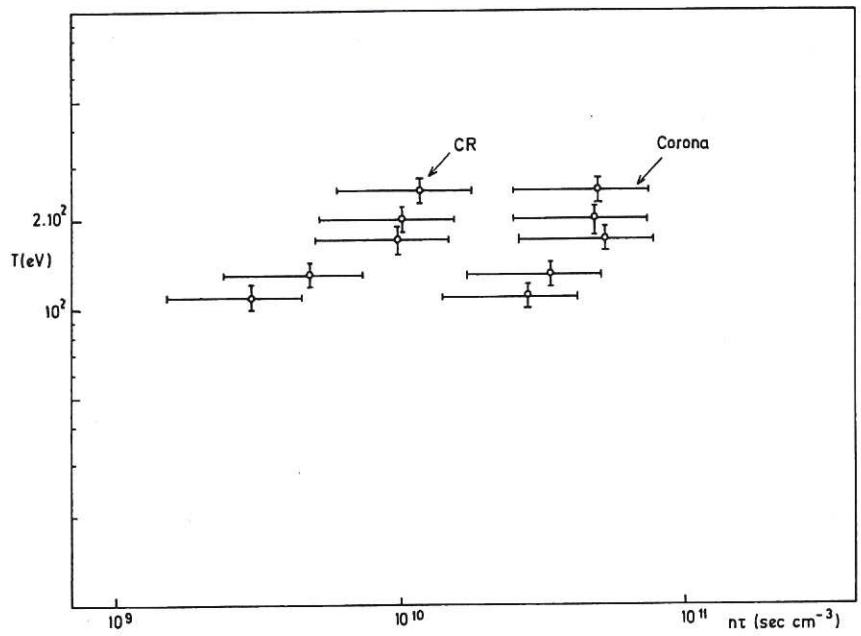

Fig 8. Product of electron density and heating time $N_e\tau$, cm^{-3} sec, calculated from the observed ion population ratios using time-dependent coronal and collisional radiative ionisation models.

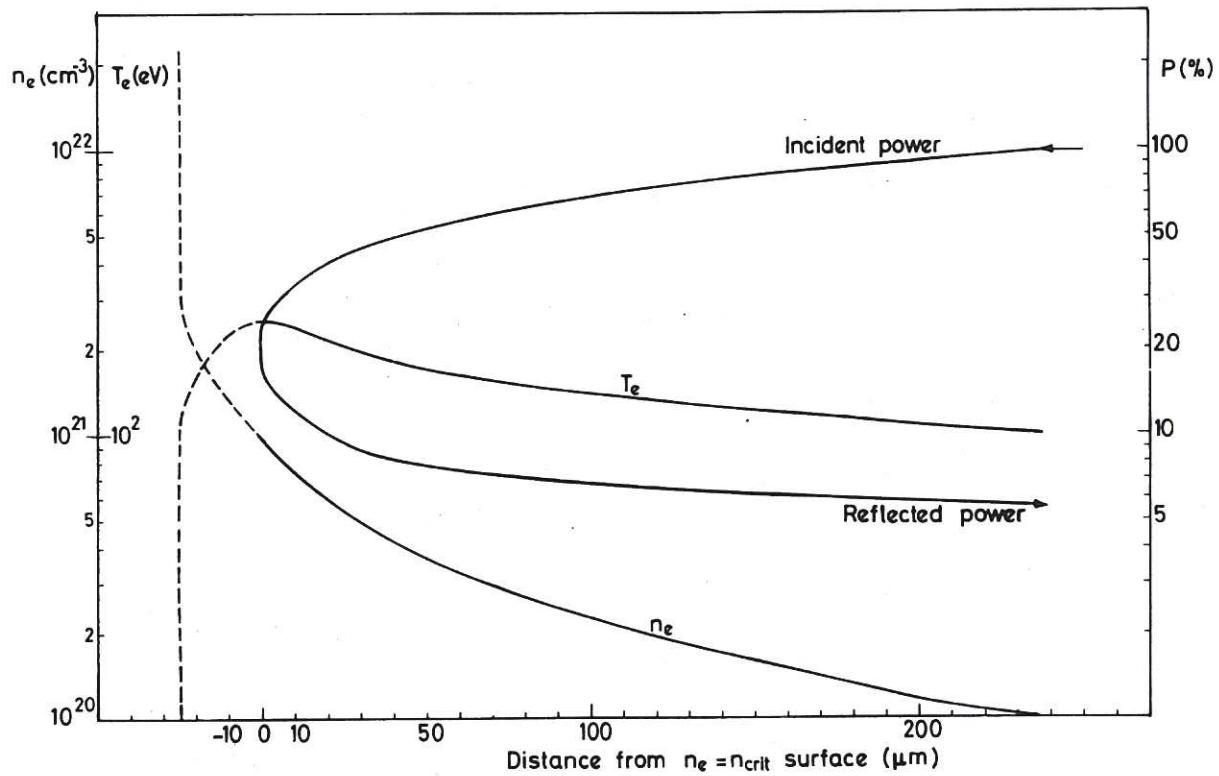

Fig 9. Calculation of the light flux intensity in the plasma produced at a polyethylene surface irradiated by 10^{12} watts cm^{-2} of 1.06 micron laser light. The density and temperature profiles normal to the surface are as for Figure 4.